

A coupled, two-dimensional hydrodynamic-marsh model with biological feedback



Karim Alizad^{a,*}, Scott C. Hagen^b, James T. Morris^c, Peter Bacopoulos^d, Matthew V. Bilskie^b, John F. Weishampel^e, Stephen C. Medeiros^a

^a University of Central Florida, Department of Civil, Environmental, and Construction Engineering, 4000 Central Florida Blvd., PO Box 162450, Orlando, FL 32816, USA

^b Louisiana State University, Department of Civil, and Environmental Engineering/Center for Computation & Technology, Baton Rouge, LA 70803, USA

^c Department of Biological Sciences and Belle W. Baruch Institute, University of South Carolina, Columbia, SC 29208, USA

^d University of North Florida, School of Engineering, 1 UNF Drive, Building 50, Room 3000, Jacksonville, FL 32224, USA

^e University of Central Florida, Department of Biology, Biological Sciences Bldg., 4110 Libra Drive, Orlando, FL 32816, USA

ARTICLE INFO

Article history:

Received 22 September 2015

Received in revised form 21 January 2016

Accepted 22 January 2016

Available online 13 February 2016

Keywords:

Salt marsh

Hydrodynamics

Timucuan marsh system

Sea-level rise

Marsh equilibrium model (MEM)

Hydro-MEM model

ABSTRACT

A spatially-explicit model (Hydro-MEM model) that couples astronomic tides and *Spartina alterniflora* dynamics was developed to examine the effects of sea-level rise on salt marsh productivity in northeast Florida. The hydrodynamic component of the model simulates the hydroperiod of the marsh surface driven by astronomic tides and the marsh platform topography, and demonstrates biophysical feedback that non-uniformly modifies marsh platform accretion, plant biomass, and water levels across the estuarine landscape, forming a complex geometry. The marsh platform accretes organic and inorganic matter depending on the sediment load and biomass density which are simulated by the ecological-marsh component (MEM) of the model and are functions of the hydroperiod. Two sea-level rise projections for the year 2050 were simulated: 11 cm (low) and 48 cm (high). Overall biomass density increased under the low sea-level rise scenario by 54% and declined under the high sea-level rise scenario by 21%. The biomass-driven topographic and bottom friction parameter updates were assessed by demonstrating numerical convergence (the state where the difference between biomass densities for two different coupling time steps approaches a small number). The maximum coupling time steps for low and high sea-level rise cases were calculated to be 10 and 5 years, respectively. A comparison of the Hydro-MEM model with a parametric marsh equilibrium model (MEM) indicates improvement in terms of spatial pattern of biomass distribution due to the coupling and dynamic sea-level rise approaches. This integrated Hydro-MEM model provides an innovative method by which to assess the complex spatial dynamics of salt marsh grasses and predict the impacts of possible future sea level conditions.

© 2016 Elsevier B.V. All rights reserved.

1. Introduction

Coastal salt marsh systems provide intertidal habitats for many species (Halpin, 2000; Pennings and Bertness, 2001), many of which (e.g., crabs and fish) have significant commercial importance. Marshes also protect shorelines by dissipating wave energy and increasing friction, processes which subsequently decrease flow energy (Knutson, 1987; Leonard and Luther, 1995; Möller and Spencer, 2002; Shepard et al., 2011). Salt marsh communities are classic examples of systems that are controlled by and in turn influence physical processes (Silliman and Bertness, 2002).

Studying the dynamics of salt marshes, which are characterized by complex inter-relationships between physics and biology (Townend et al., 2011), requires the coupling of seemingly disparate models to capture their sensitivity and feedback processes (Reed, 1990). Furthermore, coastal ecosystems need to be examined using dynamic models, because biophysical feedbacks change topography and bottom friction with time (Jørgensen and Fath, 2011a). Such coupled models allow researchers to examine marsh responses to natural or anthropogenic changes in environmental conditions. The models can be divided into landscape scale and fine scale models based on the scales for projecting vegetation productivity. Ecosystem-based landscape models are designed to lower the computational expense by expanding the resolution to the order of kilometers and simplifying physical processes between ecosystem units (Fagherazzi et al., 2012). These models connect

* Corresponding author. Tel.: +1 4078234843.

E-mail address: k.alizad@knights.ucf.edu (K. Alizad).

different drivers including hydrology, hydrodynamics, water nutrients, environmental inputs and integrate them in a large scale model (Clough et al., 2010; Costanza and Ruth, 1998; Costanza et al., 1990; Craft et al., 2008; Fitz et al., 1996; Martin et al., 2002, 2000; Park et al., 1986, 1989; Reyes et al., 2000; Sklar et al., 1985). However, fine scale models with resolutions on the order of meters can provide more realistic results by including different feedback mechanisms. Most relevant to this work is their ability to model the response in marsh productivity to a change in forcing mechanisms (e.g., sea-level rise-SLR) (Allen, 1997; Hagen et al., 2013; Kirwan and Murray, 2007; Marani et al., 2013; Mariotti and Fagherazzi, 2010; Morris et al., 2002; Mudd et al., 2004; Reed, 1995; Schile et al., 2014; Stralberg et al., 2011; Tambroni and Seminara, 2012; Temmerman et al., 2003).

Previous studies have shown that salt marshes possess biological feedbacks that change relative marsh elevation by accreting organic and inorganic material (Bastian et al., 2012; Kirwan and Guntenspergen, 2012; Morris et al., 2002; Patrick and DeLaune, 1990; Reed, 1995; Turner et al., 2000). SLR also will cause salt marshes to transgress, but extant marshes may be unable to accrete at a sufficient rate in response to high SLR (Donnelly and Bertness, 2001; Warren and Niering, 1993) leading to their complete submergence and loss (Nyman et al., 1993).

Salt marsh systems adapt to changing mean sea level through continuous adjustment of the marsh platform elevation toward an equilibrium (Morris et al., 2002). Based on long-term measurements of sediment accretion and marsh productivity, Morris et al. (2002) developed the Marsh Equilibrium Model (MEM) that links sedimentation, biological feedback, and the relevant time scale for SLR. Marsh equilibrium theory holds that a dynamic equilibrium exists, and that marshes are continuously moving in the direction of that equilibrium. MEM uses a polynomial formulation for salt marsh productivity and accounts explicitly for inputs of suspended sediments and implicitly for the in situ input of organic matter to the accreting salt marsh platform. The coupled model presented in this manuscript incorporates biological feedback by including the MEM accretion formulation as well as implementing a friction coefficient effect that varies between subtidal and intertidal states. The resulting model not only has the capability of capturing biophysical feedback that modifies relative elevation, but it also includes the biological feedback on hydrodynamics.

Since the time scale for SLR is on the order of decades to centuries, models that are based on long-term measurements, like MEM, are able to capture a fuller picture of the governing long-term processes than physical models that use temporary physical processes to extrapolate long-term results (Fagherazzi et al., 2012). MEM has been applied to a number of investigations on the interaction of hydrodynamics and salt marsh productivity. Mudd et al. (2004) used MEM coupled with a one-dimensional hydrodynamic component to investigate the effect of SLR on sedimentation and productivity in salt marshes at the North Inlet estuary, South Carolina. MEM has also been used to simulate the effects of vegetation on sedimentation, flow resistance, and channel cross section change (D'Alpaos et al., 2006), as well as in a three-dimensional model of salt marsh accretion and channel network evolution based on a physical model for sediment transport (Kirwan and Murray, 2007). Hagen et al. (2013) coupled a two-dimensional hydrodynamic model with the zero-dimensional biomass production formula of Morris et al. (2002) to capture SLR effects on biomass density and simulated human-enhanced marsh accretion.

Coupling a two-dimensional hydrodynamic model with a point-based parametric marsh model that incorporates biological feedback, such as MEM, has not been previously achieved. Such a model is necessary because results from short-term limited hydrodynamic studies cannot be used for long-term or extreme events in ecological and sedimentary interaction applications. Hence, there

is a need for integrated models, which incorporate both hydrodynamic and biological components for long time scales (Thomas et al., 2014). Additionally, models that ignore the spatial variability of the accretion mechanism may not accurately capture the dynamics of a marsh system (Thorne et al., 2014), and it is important to model the distribution at the correct scale for spatial modeling (Jørgensen and Fath, 2011b).

Ecological models that integrate physics and biology provide a means of examining the responses of coastal systems to various possible scenarios of environmental change. D'Alpaos et al. (2007) employed simplified shallow water equations in a coupled model to study SLR effects on marsh productivity and accretion rates. Temmerman et al. (2007) applied a more physically complicated shallow water model to couple it with biological models to examine landscape evolution within a limited domain. These coupled models have shown the necessity of the interconnection between physics and biology; however, the applied physical models were simplified or the study area was small. This paper presents a practical framework with a novel application of MEM that enables researchers to forecast the fate of coastal wetlands and their responses to SLR using a physically more complicated hydrodynamic model and a larger study area. The coupled Hydro-MEM model is based on the model originally presented by Hagen et al. (2013). This model has since been enhanced to include: spatially dependent marsh platform accretion, a bottom friction roughness coefficient (Manning's n) using temporal and spatial variations in habitat state, a "coupling time step" to incrementally advance and update the solution, and changes in biomass density and hydroperiod via biophysical feedbacks. The presented framework can be employed in any estuary or coastal wetland system to assess salt marsh productivity regardless of tidal range by updating an appropriate biomass curve for the dominant salt marsh species in the estuary. In this study, the coupled model was applied to the Timucuan marsh system located in northeast Florida under high and low SLR scenarios. The objectives of this study were to (1) develop a spatially-explicit model by linking a hydrodynamic-physical model and MEM using a coupling time step and (2) assess a salt marsh system long-term response to projected SLR scenarios.

2. Methods

2.1. Study area

The study area is the Timucuan salt marsh, located along the lower St. Johns River in Duval County in northeastern Florida (Fig. 1). The marsh system is located to the north of the lower 10–20 km of the St. Johns River, where the river is engineered and the banks are hardened for support of shipping traffic and port utility. The creeks have changed little from 1929 to 2009 based on surveyed data from National Ocean Service (NOS) and the United States Army Corps of Engineers (USACE), which show the creek layout to have remained essentially the same since 1929. The salt marsh of the Timucuan preserve, which was designated the Timucuan Ecological and Historic Preserve in 1988, is among the most pristine and undisturbed marshes found along the southeastern United States seaboard (United States National Park Service (Denver Service Center), 1996). Maintaining the health of the approximately 185 square km of salt marsh, which cover roughly 75% of the preserve, is important for the survival of migratory birds, fish, and other wildlife that rely on this area for food and habitat.

The primary habitats of these wetlands are salt marshes and the tidal creek edges between the north bank and Sisters Creek are dominated by low marsh, where *Spartina alterniflora* thrives (DeMort, 1991). A sufficient biomass density of *S. alterniflora* in the

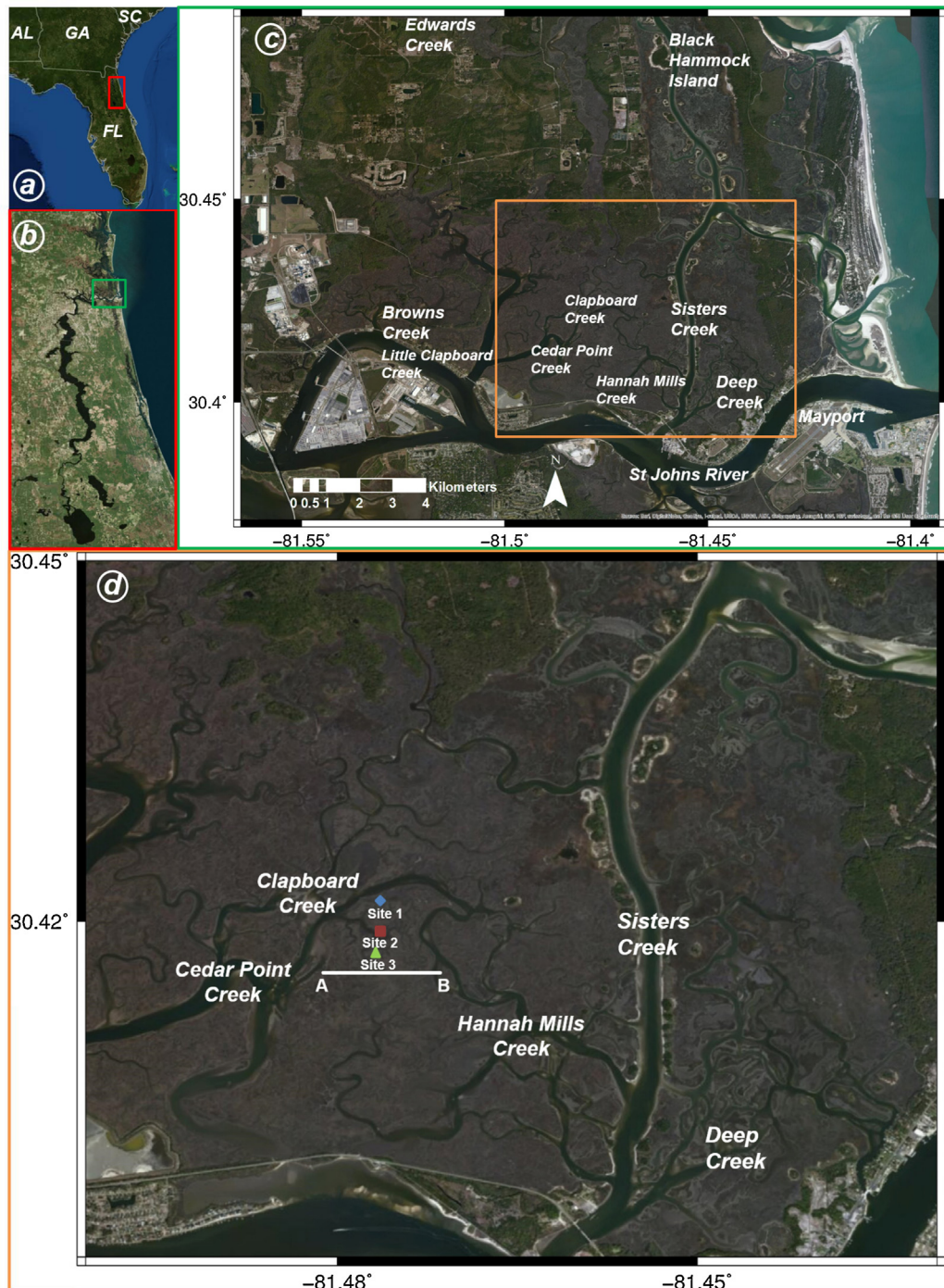


Fig. 1. Study area and progressive insets. (a) Location of St. Johns river; (b) Location of Timucuan salt marsh system and lower St. Johns river; (c) Timucuan salt marsh system and tidal creeks. (d) Sub-region of Timucuan including the location of example transect AB and three biomass sample sites. Site 1 (blue) is in a low biomass productivity region, site 2 (red) is in a medium biomass productivity region, and site 3 (green) is in a high biomass productivity region. The maps are screen captures of world imagery in ArcGIS (ESRI, 2012) (For interpretation of the references to color in this figure legend, the reader is referred to the web version of this article.).

marsh is integral to its survival, as the grass aids in shoreline protection, erosion control, filtering of suspended solids, and nutrient uptake of the marsh system (Bush and Houck, 2002). *S. alterniflora* covers most of the southern part of the watershed and east of Sisters Creek up to the primary dunes on the north bank, and is also the dominant species on the Black Hammock barrier island (DeMort, 1991). The low marsh is the more tidally vulnerable region of the study area. Our focus is on the areas that are directly exposed to SLR and where *S. alterniflora* is dominant. However, we also extended our salt marsh study area 11 miles to the south, 17 miles to the

north, and 18 miles to the west of the mouth of the St. Johns River. The extension of the model boundary allows enough space to study the potential for salt marsh migration.

2.2. Overall model description

The flowchart shown in Fig. 2 illustrates the dynamic coupling of the physical and biological processes in the model. The framework to run the Hydro-MEM model consists of two main elements: the hydrodynamic model, and a marsh model with biological

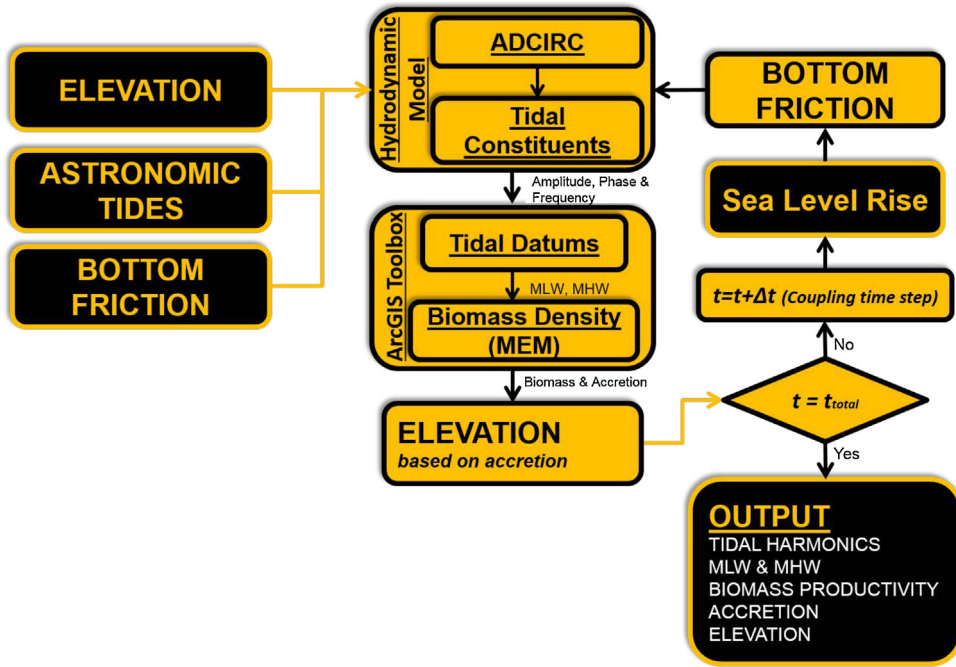


Fig. 2. Hydro-MEM model flowchart. The black boxes show the parameters that are not being changed and the gold boxes are the parameters that are being changed through simulation. The two main elements are the big gold boxes which are labeled as hydrodynamic model and ArcGIS toolbox. The black boxes on the left represent the initial conditions.

feedback (MEM) in the form of an ArcGIS toolbox. The two model components provide inputs for one another at a specified time step within the loop structure, referred to as the coupling time step. The coupling time step refers to the length of the time interval between updating the hydrodynamics based on the output of MEM, which was always integrated with an annual time step. The length of the coupling time step (Δt) governs the frequency of exchange of information from one model component to the other. The choice of coupling time step size affects the accuracy and computational expense of the Hydro-MEM model which is an important consideration if extensive areas are simulated. The model's initial conditions include astronomic tides, bottom friction, and elevation, which consist of the marsh surface elevations, creek geometry, and sea level. The hydrodynamic model is then run using the initial conditions and its results are processed to derive tidal constituents.

The tidal constituents are fed into the ArcGIS toolbox, which contains two components that were designed to work independently. The "Tidal Datums" element of the ArcGIS toolbox computes Mean Low Water (MLW) and Mean High Water (MHW) in regions that were always classified as wetted during the hydrodynamic simulation. The second component of the toolbox, "Biomass Density," uses the MLW and MHW calculated in the previous step and extrapolates those values across the marsh platform using the Inverse Distance Weighting (IDW) method of extrapolation in ArcGIS (i.e., from the areas that were continuously wetted during the hydrodynamic simulation), computes biomass density for the marsh platform, and establishes a new marsh platform elevation based on the computed accretion.

The simulation terminates and outputs the final results if the target time has been reached, otherwise time is incremented by the coupling time step, data are transferred and model inputs are modified, and another incremental simulation is performed. After each time advancement of the MEM and after updating the topography, the hydrodynamic model is re-initialized using the current elevations, water levels, and updated bottom friction parameters calculated in the previous iteration.

The size of the coupling time step, i.e. the time elapsed in executing MEM before updating the hydrodynamic model, was selected based on desired accuracy and computational expense. The coupling time step was adjusted in this work to minimize numerical error associated with biomass calculations (the difference between using two different coupling time steps) while also minimizing the run time.

2.2.1. Hydrodynamic model

We used the two-dimensional, depth-integrated Advanced CIRCulation (ADCIRC) finite element model to simulate tidal hydrodynamics (Luettich et al., 1992). ADCIRC is one of the main components of the Hydro-MEM model due to its capability to simulate the highly variable tidal response throughout the creeks and marsh platform. ADCIRC solves the shallow water equations for water levels and currents using continuous Galerkin finite elements in space. ADCIRC based models have been used extensively to model long wave processes such as astronomic tides and hurricane storm surge (Bacopoulos and Hagen, 2009; Bunya et al., 2010) and SLR impacts (Atkinson et al., 2013; Bilske et al., 2014). A value-added feature of using ADCIRC within the Hydro-MEM model is its ability to capture a two-dimensional field of the tidal flow and hydroperiod within the intertidal zone. ADCIRC contains a robust wetting and drying algorithm that allows elements to turn on (wet) or turn off (dry) during run-time, enabling the swelling of tidal creeks and overtopping of channel banks (Medeiros and Hagen, 2013). A least-squares harmonic analysis routine within ADCIRC computes the amplitudes and phases for a specified set of tidal constituents at each computational point in the model domain (global water levels). The tidal constituents are then sent to the ArcGIS toolbox for further processing.

Full hydrodynamic model description including elevation sources and boundary conditions can be found in Bacopoulos et al. (2012) and Hagen et al. (2013). The model is forced with the seven dominating tidal constituents along the open ocean boundary located on the continental shelf that account for more than 90% of the offshore tidal activity (Bacopoulos et al., 2012; Hagen

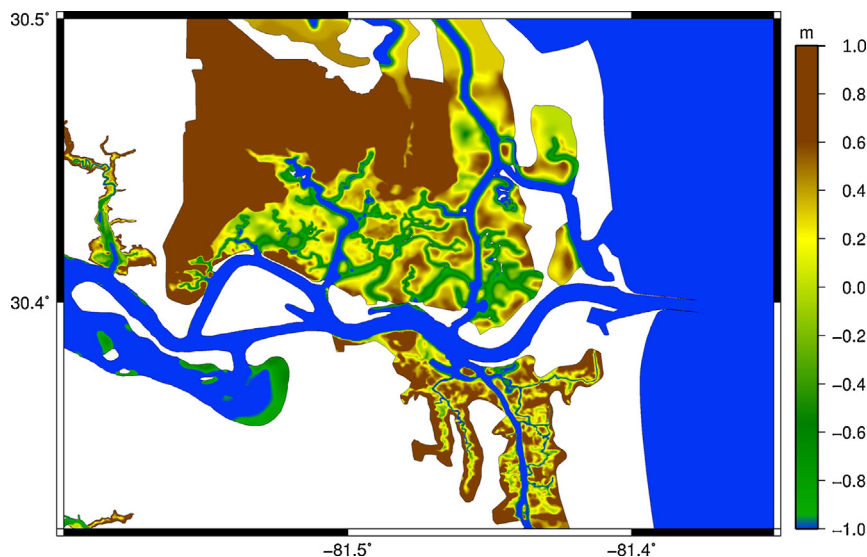


Fig. 3. ADCIRC model input of the Timucuan salt marsh surface elevations. Elevations are referenced to NAVD88 in meters with blue representing water depths greater than 1 m, greens indicating depths between 0 m and 1 m, and yellows and browns representative of elevations above 0 m NAVD88 (For interpretation of the references to color in this figure legend, the reader is referred to the web version of this article.).

et al., 2013). Placement of the offshore tidal boundary allows tides to propagate through the domain and into the tidal creeks and intertidal zones, and simulate non-linear interactions that occur in the tidal flow.

To model future conditions, sea level was increased by applying an offset of the initial sea surface equal to the SLR across the model domain to the initial conditions. Previous studies introduced SLR by applying an additional tidal constituent to the offshore boundary (Hagen et al., 2013). Both methods produce an equivalent solution; however, we offset the initial sea surface across the entire domain as the method of choice in order to reduce computational time.

There is no accepted method to project SLR at the local scale (Parris et al., 2012); however, a tide gauge analysis performed in Florida using three different methods gave a most probable range of rise between 0.11 and 0.36 m from present to the year 2080 (Walton, 2007). The U.S. Army Corps of Engineers (USACE) developed low, intermediate, and high SLR projections at the local scale, based on long-term tide gage records (http://www.corpsclimate.us/ccaceslcurves_nn.cfm). The low curve follows the historic trend of SLR and the intermediate and high curves use the National Research Council (NRC) curves (United States Army Corps of Engineers (USACE), 2011). Both methodologies account for local subsidence. We based our SLR scenarios on the USACE projections at Mayport, FL (Fig. 1c), which accelerates to 11 cm and 48 cm for the low and high scenarios, respectively, in the year 2050. The low and high SLR scenarios display linear and nonlinear trends, respectively and using the time step approach helps to capture the rate of SLR in the modeling.

The hydrodynamic model uses Manning's n coefficients for bottom friction, which have been assessed for present-day conditions of the lower St. Johns River (Bacopoulos et al., 2012). Bottom friction must be continually updated by the model due to temporal changes in the SLR and biomass accretion. To compute Manning's n at each coupling time step, the Hydro-MEM model utilizes the wet/dry area output of the hydrodynamic model as well as biomass density and accreted marsh platform elevation to find the regions that changed from marsh (dry) to channel (wet). This process is a part of the biofeedback process in the model: Manning's n is adjusted using the accretion, which changes the hydrodynamics, which in turn changes the biomass density in the next time step. The hydrodynamic model, along with the main digital elevation model

(Fig. 3) and bottom friction parameter (Manning's n) inputs, was previously validated in numerous studies (Bacopoulos et al., 2009, 2012, 2011; Giardino et al., 2011; Hagen et al., 2013) and specifically Hagen et al. (2013) validated the MLW and MHW generated by this model.

2.2.2. ArcGIS toolbox

This element of the Hydro-MEM model is designed as a user interface toolbox in ArcGIS (ESRI, 2012). The toolbox consists of two separate tools that were coded in Python v2.7. The first, "Tidal Datums," uses tidal constituents from the preceding element of the Hydro-MEM model loop, the hydrodynamic model, to generate MLW and MHW in the river and tidal creeks. MLW and MHW represent the average low and high tides at a point (Hagen et al., 2013). The flooding frequency and duration are considered in the calculation of MLW and MHW. These values are necessary for the MEM-based tool in the model. The Tidal Datums tool produces raster files of MLW and MHW using the data from ADCIRC simulation and a 10 m Digital Elevation Model (DEM). These feed into the second tool, "Biomass Density," to calculate MLW and MHW within the marsh areas that were not continuously wet during the ADCIRC simulation, which is done by interpolating MLW and MHW values from the creeks and river areas across the marsh platform using IDW. This interpolation technique is necessary because very small creeks that are important in flooding the marsh surface are not resolved in the hydrodynamic model. IDW calculates MLW and MHW at each computational point across the marsh platform based on its distance from the tidal creeks, where the number of the nearest sample points for the IDW interpolation based on the default setting in ArcGIS is twelve. This method was used in this work for the marsh interpolation due to its accuracy and acceptable computational time. The method produces lower water levels for points farther from the source, which in turn results in lower sedimentation and accretion in the MEM-based part of the model. Interpolated MLW and MHW, biomass productivity, and accretion are displayed as rasters in ArcGIS. The interpolated values of MLW and MHW in the marsh are used by MEM in each raster cell to compute the biomass density and accretion rate across the marsh platform.

The zero-dimensional implementation of MEM has been demonstrated to successfully capture salt marsh response to SLR

(Morris, 2015; Morris et al., 2002). MEM predicts two salt marsh variables: biomass productivity and accretion rate. These processes are related; the organic component of the accretion is dependent on biomass productivity, and the updated marsh platform elevation is generated using the computed accretion rate. The coupling of the two parts of MEM is incorporated dynamically in the Hydro-MEM model. MEM approximates salt marsh productivity as a parabolic function

$$B = aD + bD^2 + c \quad (1)$$

where B is the biomass density (g m^{-2}), $a = 1000 \text{ g m}^{-2}$, $b = -3718 \text{ g m}^{-2}$, and $c = 1021 \text{ g m}^{-2}$ are coefficients derived from bioassay data collected at North Inlet, SC (Morris et al., 2013) and where the variable D is the non-dimensional depth, given by

$$D = \frac{\text{MHW} - E}{\text{MHW-MLW}} \quad (2)$$

and variable E is the relative marsh surface elevation (NAVD 88). Relative elevation is a proxy for other variables that directly regulate growth, such as soil salinity (Morris, 1995) and hypoxia, and Eq. (1) actually represents a slice through n-dimensional niche space (Hutchinson, 1957).

The coefficients a , b , and c may change with marsh species, estuary type (fluvial, marine, mixed), climate, nutrients, and salinity (Morris, 2007), but Eq. (1) should be independent of tide range because it is calibrated to dimensionless depth D , consistent with the meta-analysis of Mckee and Patrick (1988) documenting a correlation between the growth range of *S. alterniflora* and mean tide range. The coefficients a , b , and c in Eq. (1) give a maximum biomass of 1088 g m^{-2} , which is generally consistent with biomass measurements from other southeastern salt marshes (Dame and Kenny, 1986; Darby and Turner, 2008; Hopkinson et al., 1980; Schubauer and Hopkinson, 1984), and since our focus is on an area where *S. alterniflora* is dominant, these constants are used. Additionally, because many tidal marsh species occupy a vertical range within the upper tidal frame, but sorted along a salinity gradient, the model is able to qualitatively project the wetland area coverage including other marsh species in low, medium, and high productivity. The framework has the capability to be applied to other sites with different dominant salt marsh species by using experimentally-derived coefficients to generate the biomass curves (Kirwan and Guntenspergen, 2012).

The first derivative of the biomass density function with respect to non-dimensional depth is a linear function, which will be used in analyzing the Hydro-MEM model results, is given by

$$\frac{dB}{dD} = 2bD + a \quad (3)$$

The first derivative values are close to zero for the points around the optimal point of the biomass density curve. These values become negative for the points on the right (sub-optimal) side and positive for the points on the left (super-optimal) side of the biomass density curve.

The accretion rate determined by MEM is a positive function based on organic and inorganic sediment accumulation (Morris et al., 2002). These two accretion sources, organic and inorganic, are necessary to maintain marsh productivity against rising sea level; otherwise marshes might become submerged (Baustian et al., 2012; Blum and Roberts, 2009; Nyman et al., 2006). Sediment accretion is a function of the biomass density in the marsh and relative elevation. Inorganic accretion (i.e., mineral sedimentation) is influenced by the biomass density, which affects the ability of the marsh to 'trap' sediments (Mudd et al., 2010). Inorganic sedimentation also occurs as salt marshes impede flow by increasing friction, which enhances sediment deposition on the marsh platform (Leonard and Croft,

2006; Leonard and Luther, 1995). The linear function developed by Morris et al. (2002) for the rate of total accretion is given by

$$\frac{dY}{dt} = (q + kB)D \quad \text{for } D > 0 \quad (4)$$

where dY is the total accretion (cm/yr), dt is the time interval, q represents the inorganic contribution to accretion from the suspended sediment load and k represents the organic and inorganic contributions due to vegetation. The values of the constants q (0.0018) and k (2.5×10^{-5}) are from a fit of MEM to a time-series of marsh elevations at North Inlet (Morris et al., 2002) modified for a high sedimentary environment. These constants take both autochthonous organic matter and trapping of allochthonous mineral particles into account for biological feedback. The accretion rate is positive for salt marshes below MHW; when $D < 0$ no accumulation of sediments will occur for salt marshes above MHW (Morris, 2007). The marsh platform elevation change is then calculated using the following equation

$$Y(t + \Delta t) = Y(t) + dY \quad (5)$$

where the marsh platform elevation Y is raised by dY meters every Δt years.

3. Results

3.1. Coupling time step

In this study, coupling time steps of 50, 10, and 5 years were used for both the low and high SLR scenarios. The model was run for one 50-year coupling time step, five 10-year coupling time steps, and ten 5-year coupling time steps for each SLR scenario. The average differences for biomass density in Timucuan marsh between using one 50-year coupling time step and five 10-year coupling time steps for low and high SLR scenarios were 37 and 57 g m^{-2} , respectively. Decreasing the coupling time step to 5 years indicated convergence within the marsh system when compared to a 10-year coupling time step (Table 1). The average difference for biomass density between using five 10-year coupling time steps and ten 5-year coupling time steps in the same area for low and high SLR were 6 and 11 g m^{-2} , which implied convergence using smaller coupling time steps. The Hydro-MEM model did not fully converge using a coupling time step of 10 years for the high SLR scenario, and a 5 year coupling time step was required (Table 1) because of the acceleration in rate of SLR. However, the model was able to simulate reasonable approximations of low, medium, or high productivity of the salt marshes when applying a single coupling time step of 50 years when SLR is small and linear. For this case, the model was run for the current condition and the feedback mechanism is subsequently applied using 50-year coupling time step. The next run produces the results for salt marsh productivity after 50 years using the SLR scenario.

3.2. Hydrodynamic results

MLW and MHW demonstrated spatial variability throughout the creeks and over the marsh platform. The water surface across the estuary varied from -0.85 m to -0.3 m (NAVD 88) for MLW and from 0.65 m to 0.85 m for MHW in the present day simulation (Fig. 4a and d). The range and spatial distribution of MHW and MLW exhibited a non-linear response to future SLR scenarios. Under the low SLR (11 cm) scenario, MLW ranged from -0.74 m in the ocean to -0.25 m in the creeks (Fig. 4b), while MHW varied from 1 m to 0.75 m (Fig. 4e). Under the high SLR (48 cm) scenario, the MLW

Table 1

Model convergence as a result of various coupling time steps.

Number of coupling time steps	Coupling time step (years)	Biomass density for a sample point* at low SLR (11 cm) (g m^{-2})	Biomass density for a sample point* at high SLR (48 cm) (g m^{-2})	Convergence at low SLR (11 cm)	Convergence at high SLR (48 cm)
1	50	1053	928	No	No
5	10	1088	901	Yes	No
10	5	1086	909	Yes	Yes

* The sample point is located at longitude = -81.4769 and latitude = 30.4167 .

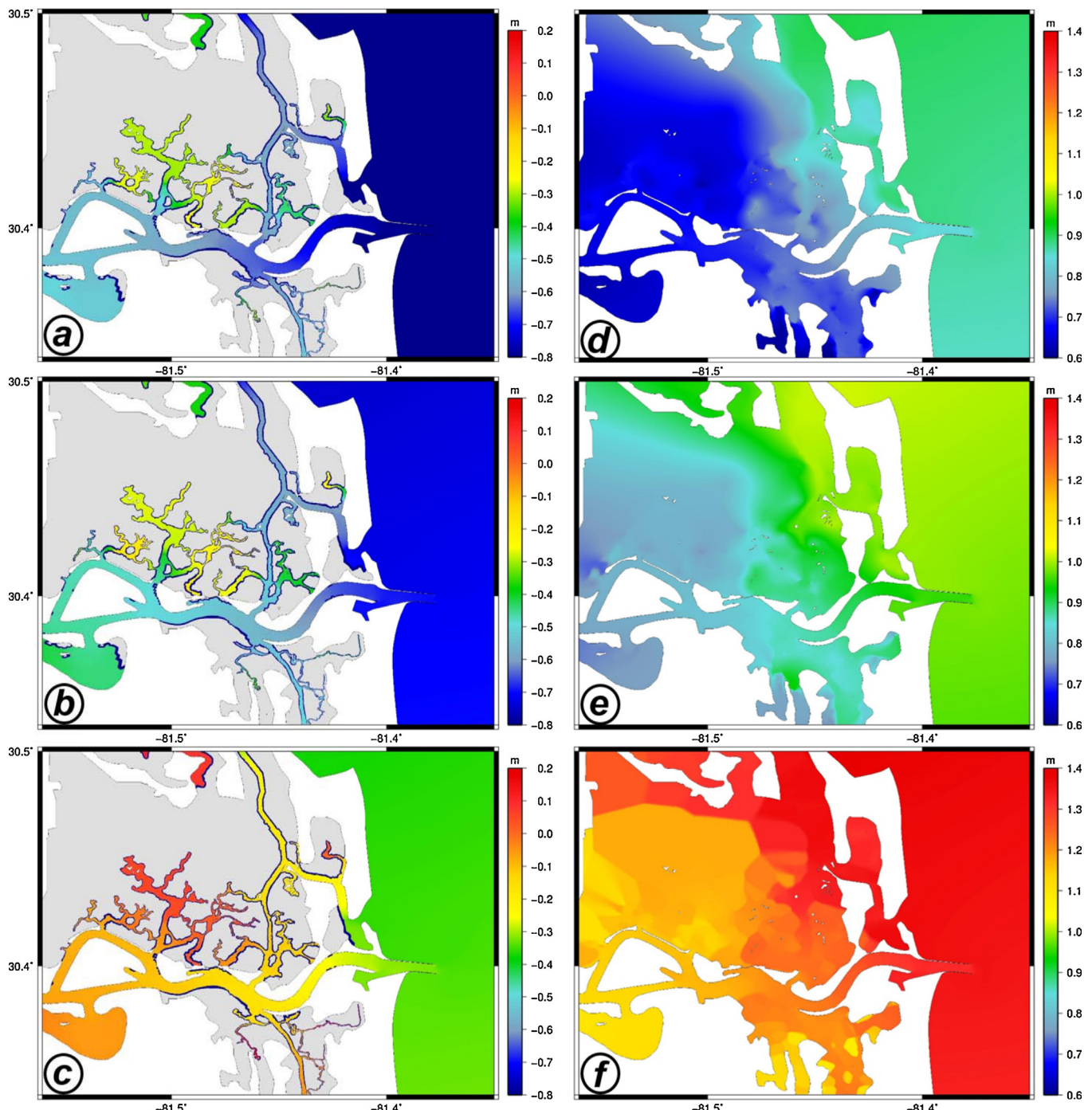


Fig. 4. MLW (left column) and MHW (right column) results for the year 2000 (a and d), and for the year 2050 under low (11 cm) (b and e) and high (48 cm) (c and f) SLR scenarios. Results are referenced to NAVD88.

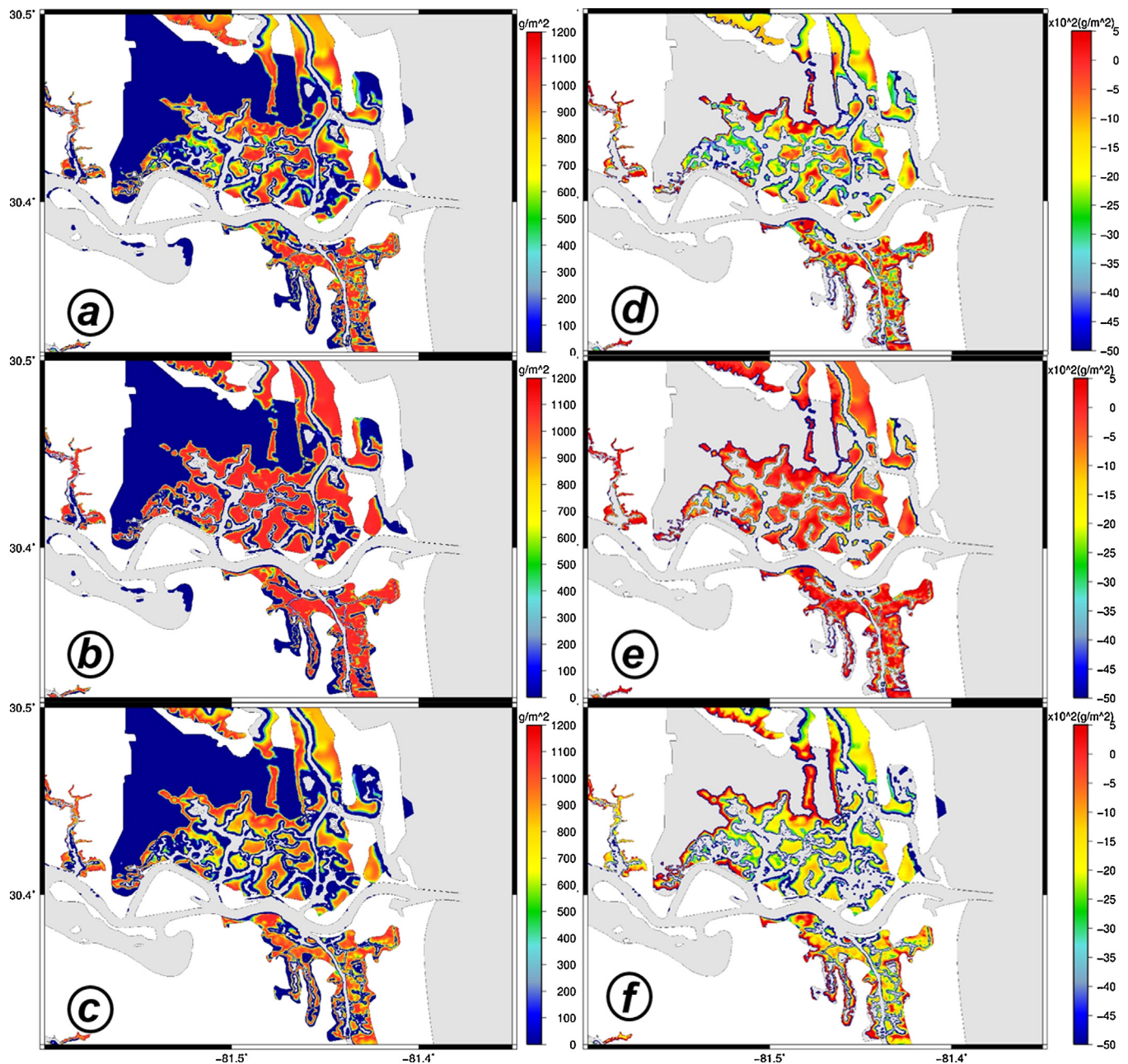


Fig. 5. Biomass density patterns (left column) and its first derivative (right column) in the Timucuan marsh system. (a) Biomass density in the year 2000; (b) Biomass density in the year 2050 under a low SLR (11 cm) scenario; (c) Biomass density in the year 2050 under a high SLR (48 cm) scenario. Dark blue represents no biomass density (0 g m^{-2}), yellows are medium biomass density ($\sim 700 \text{ g m}^{-2}$), and reds indicate biomass density of 1000 g m^{-2} or greater. (d) Biomass density first derivative in the year 2000; (e) Biomass density first derivative in the year 2050 under the low SLR (11 cm) scenario; (f) Biomass density first derivative in the year 2050 under the high SLR (48 cm) scenario. (For interpretation of the references to color in this figure legend, the reader is referred to the web version of this article.).

ranged from -0.35 m in the ocean to 0.05 m in the creeks (Fig. 4c), and from 1.35 m to 1.15 m for MHW (Fig. 4f).

The same spatial pattern of water level was exhibited on the marsh platform for both present-day and future conditions with the low SLR scenario, but with future conditions showing slightly higher values consistent with the 11 cm increase in MSL (Fig. 4d and e). The MHW values in both cases were within the same range as those in the creeks. However, the spatial pattern of MHW changed under the high SLR scenario; the water levels in the creeks increased significantly and were more evenly distributed relative to the present-day conditions and low SLR scenario (Fig. 4d–f). As a result, the spatial variation of MHW in the creeks and marsh area was lower than that of the present in the high SLR scenario (Fig. 4f).

3.3. Marsh dynamics

Simulations of biomass density demonstrated a wide range of spatial variation in the year 2000 (Fig. 5a), and in the two future scenarios (Fig. 5b and c), depending on the pre-existing elevations of the marsh surface and their change relative to future MHW and MLW. The maps showed an increase in biomass density under low SLR in 90% of the marshes and a decrease in 80% of the areas under the high SLR scenario. The average biomass density increased from 804 g m^{-2} in the present to 994 g m^{-2} in the year 2050 with low SLR, and decreased to 644 g m^{-2} under the high SLR scenario.

Recall that the derivative of biomass density under low SLR scenario varies linearly with respect to non-dimensional depth. Fig. 6

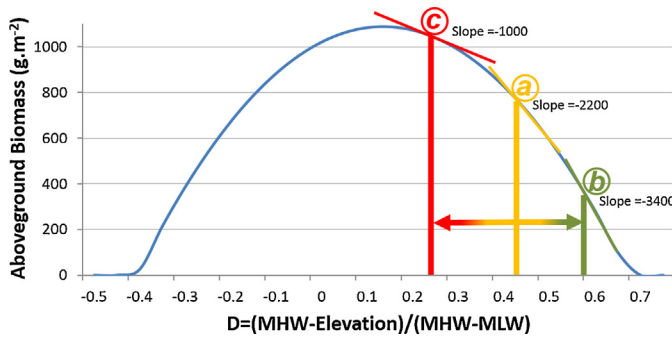


Fig. 6. Change in the biomass productivity curve under different SLR scenarios. The colors selected are based on the scale in Fig. 5. (a) is a selected geographical point from the Timucuan marsh system in the year 2000 that falls within the medium productivity range of the curve; (b) is the same geographical location (a), in the year 2050 under high SLR (48 cm) and has moved to the low productivity range of the curve; (c) is the same geographical location (a) in the year 2050 and under low SLR (11 cm) and has moved to the high productivity region.

illustrates the aboveground biomass density curve with respect to non-dimensional depth and three sample points with low, medium, and high productivity. The slope of the curve at the sample points is also shown, depicting the first derivative of biomass density. The derivative is negative if a point is located on the right side of the biomass density curve, and is positive if it is on the left side. In addition, values close to zero indicate a higher productivity, whereas large negative values indicate low productivity (Fig. 6). The average biomass density derivative under the low SLR scenario increased from -2000 g m^{-2} to -700 g m^{-2} and decreased to -2400 g m^{-2} in the high SLR case.

Sediment accretion in the marsh varied spatially and temporally under different SLR scenarios. Under the low SLR scenario (11 cm), the average salt marsh accretion totaled 19 cm or 0.38 cm per year (Fig. 7a). The average salt marsh accretion increased by 20% under the high SLR scenario (48 cm) due to an increase in sedimentation (Fig. 7b). Though the magnitudes are different, the general spatial patterns of the low and high SLR scenarios were similar.

Comparisons of marsh platform accretion, MHW, and biomass density across transect AB spanning over Cedar Point Creek, Clapboard Creek, and Hannah Mills Creek (Fig. 1d) between present and future time demonstrated that acceleration of SLR from 11 cm to 48 cm in 50 years reduced the overall biomass, but the effect depended on the initial elevation (Fig. 8a–d). Under the low SLR, accretion was maximum at the edge of the creeks, 25 to 30 cm, and

decreased to 15 cm with increasing distance from the edge of the creek (Fig. 8a). Analyzing the trend and variation of MHW between future and present across the transect under low and high SLR showed that it is not uniform across the marsh and varied with distance from creek channels and underlying topography (Fig. 8a and c). MHW increased slightly in response to a rapid rise in topography (Fig. 8a and c).

The change in MHW, which is a function of the changing hydrodynamics and marsh topography, was nearly uniform across space when SLR was high, but when SLR was low, marsh topography continued to influence MHW, which can be seen in the increase between years 2020 and 2030 (Fig. 9c and d). This is due to the accretion of the marsh platform keeping pace with the change in MHW. The change in biomass was a function of the starting elevation as well as the rate of SLR (Fig. 9e and f). When the starting marsh elevation was low, as it was for sites 1 and 2, biomass increased significantly over the 50 yr simulation, corresponding to a rise in the relative elevation of the marsh platform that moved them closer to the optimum. The site that was highest in elevation at the start, site 3, was essentially in equilibrium with sea level throughout the simulation and remained at a nearly optimum elevation (Fig. 9e). When the rate of SLR was high, the site lowest in elevation at the start, site 1, ultimately lost biomass and was close to extinction (Fig. 9f). Likewise, the site highest in elevation, site 3, also lost biomass, but was less sensitive to SLR than site 1. The site with intermediate elevation, site 2, actually gained biomass by the end of the simulation when SLR was high (Fig. 9f).

Biomass density was generally affected by rising mean sea level and varying accretion rates. A modest rate of SLR apparently benefitted these marshes, but high SLR was detrimental (Fig. 9e and f). This is further explained by looking at the derivatives. The first-derivative change of biomass density under low SLR (shaded red) demonstrated an increase toward the zero (Fig. 10). Biomass density rose to the maximum level and was nearly uniform across transect AB under the low SLR scenario (Fig. 8b), but with 48 cm of SLR biomass declined (Fig. 8d). The biomass derivative across the transect decreased from year 2000 to year 2050 under the high SLR scenario (Fig. 10), which indicated a move to the right side of the biomass curve (Fig. 6).

Comparisons between using the coupled model and MEM in isolation are given in Table 2 according to total wetland area and marsh productivity for both the coupled Hydro-MEM model and MEM. The Hydro-MEM model exhibited more spatial variation of low and medium productivity for both the low and high SLR scenarios (Fig. 11). Under the low SLR scenario there was less open water and more low and medium productivity, while under the

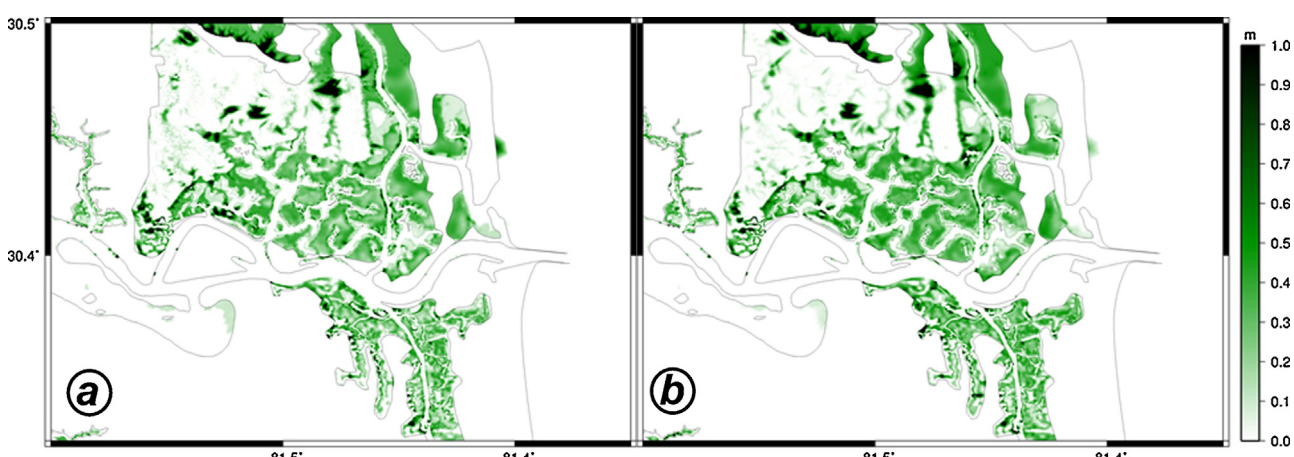


Fig. 7. Fifty years (year 2050) of salt marsh platform accretion following (a) 11 cm of SLR and (b) 48 cm of SLR.

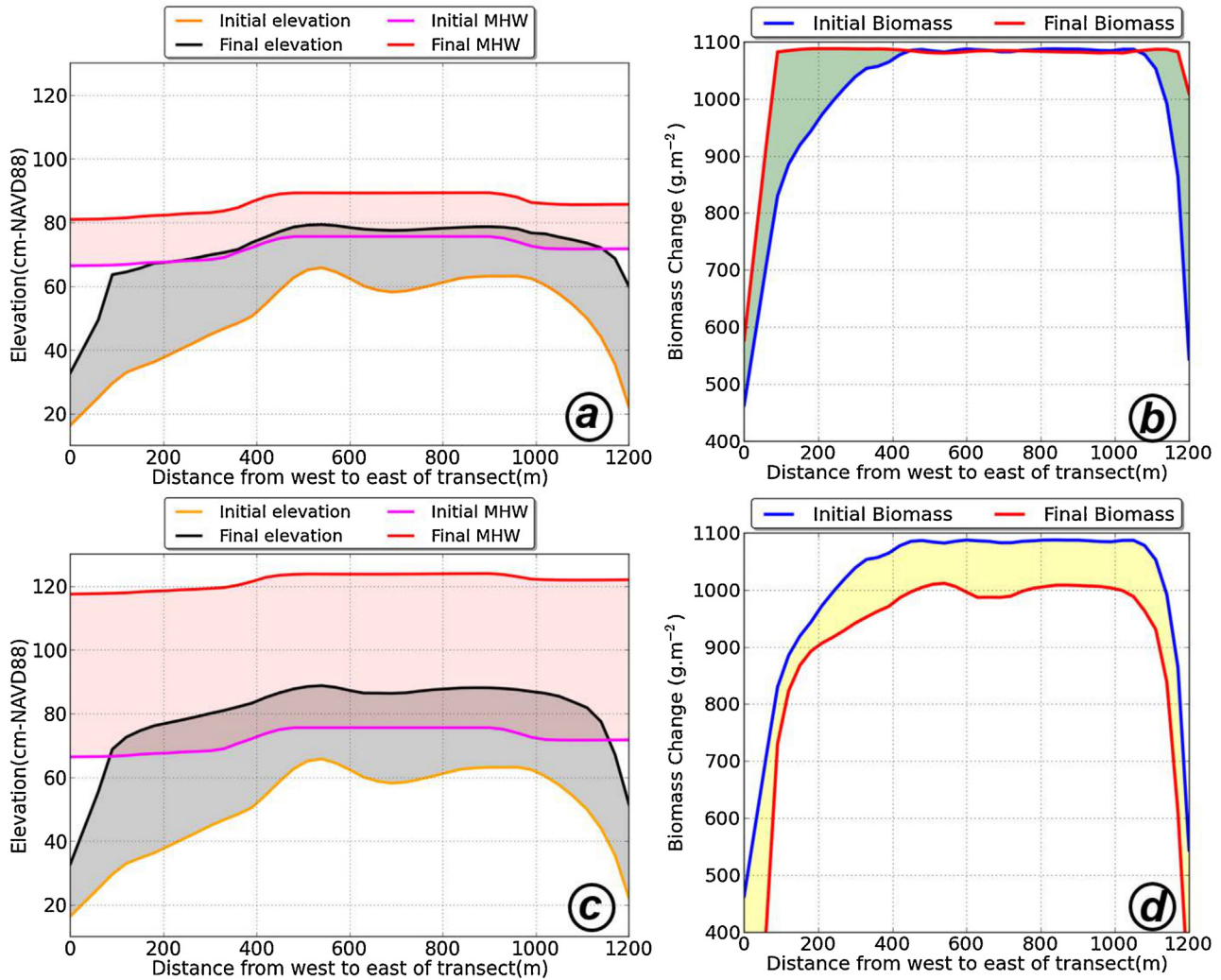


Fig. 8. Changes in elevation, MHW, and biomass along a transect (see Fig. 1d for location of transect) for the low (11 cm) (a and b) and the high (48 cm) (c and d) scenarios. (a and c) Gray shaded area shows the elevation change between years 2000 (orange line) and 2050 (black line); red shaded area represents the increase in MHW between years 2000 (magenta line) and 2050 (red line). (b and d) The dark green (yellow) shaded area shows an increase (decrease) in biomass density between years 2000 (blue line) and 2050 (red line) (For interpretation of the references to color in this figure legend, the reader is referred to the web version of this article.).

high SLR scenario there was less high productivity and more low and medium productivity.

To qualitatively validate the model result, infrared aerial imagery and land cover data from the National Land Cover Database for the year 2001 (NLCD2001) (Homer et al., 2007) were compared with the low, medium, and high productivity map (Fig. 12). Within the box marked (a) in the aerial image (leftmost figure), the boundaries for the major creeks were captured in the model results (middle figure). Additionally, smaller creeks in boxes (a)–(c) in the NLCD map (rightmost figure) also were represented well in the model results. The model identified the NLCD wetland areas corresponding to box (a) as highly productive marshes. Box (b)

highlights an area with higher elevations, shown as forest land in the aerial map, and categorized as non-wetland in the NLCD map. These regions had low or no productivity in the model results. The border of the brown (low productivity) region in the model results generally mirrors the forested area in the aerial and the non-wetland area of the NLCD data. A low elevation area identified by box (c) consists of a drowning marsh flat with a dendritic layout of shallow tidal creeks. The model identified this area as having low or no productivity, but with a productive area marsh in the south-east corner. Collectively, comparison of the model results in these areas to ancillary data demonstrates the capability of the model to realistically characterize the estuarine landscape.

Table 2

Comparisons of areal coverage by landscape classifications following 50-year simulations with high and low SLR using a coupled Hydro-MEM model vs. a direct application of a spatially-distributed marsh equilibrium model (MEM) run without hydrodynamics. The marshes with productivity less than 370 g m^{-2} are categorized as low, between 370 g m^{-2} and 750 g m^{-2} are categorized as medium, and more than 750 g m^{-2} are categorized as high productivity.

Models	Area percentage by landscape classification			
	Water	Low productivity	Medium productivity	High productivity
Hydro-MEM (low SLR)	54.4	5.2	6.3	34.1
MEM (low SLR)	62.6	1.2	1.3	34.9
Hydro-MEM (high SLR)	62.1	6.7	8.8	22.4
MEM (high SLR)	61.0	1.2	1.1	36.7

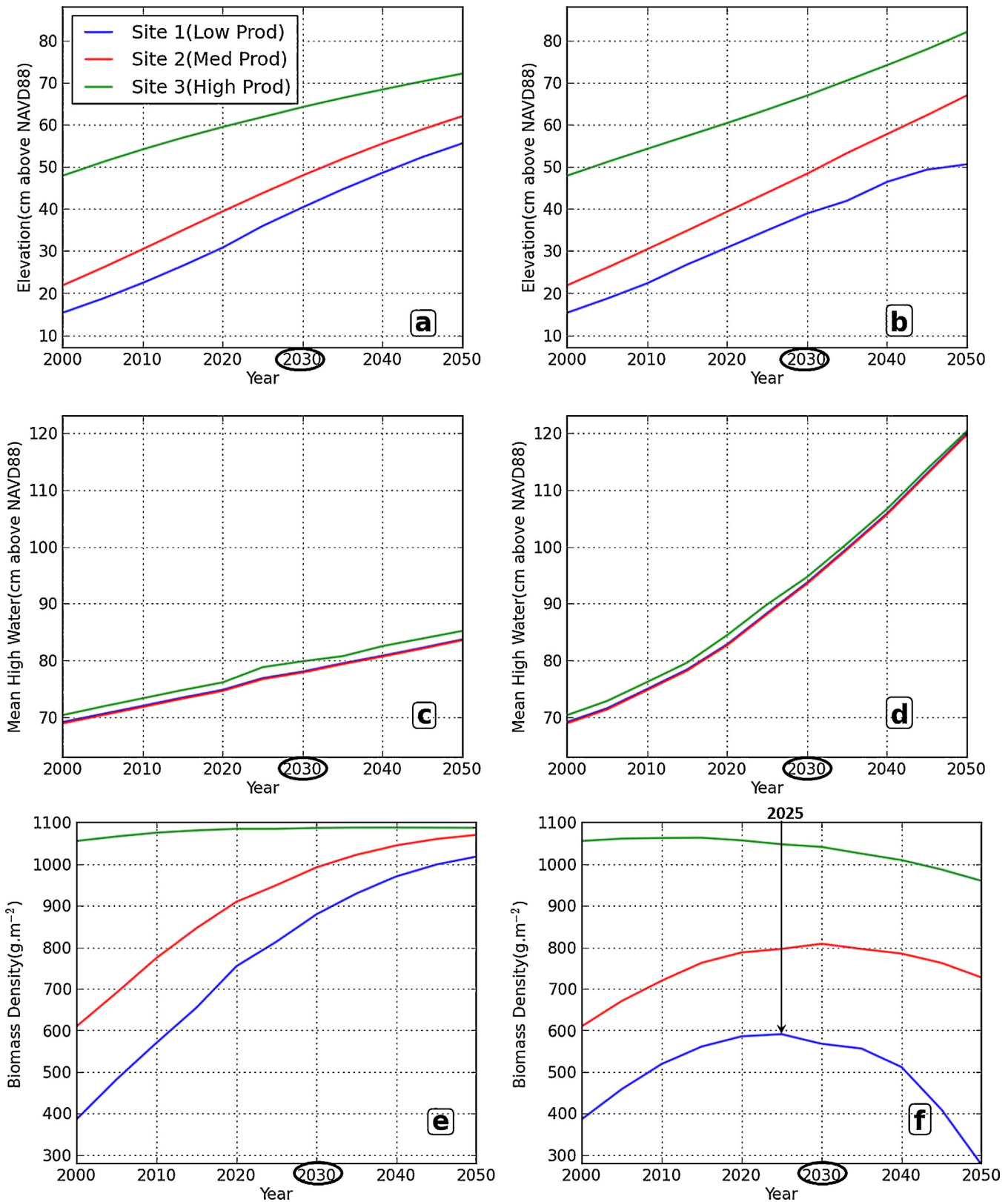


Fig. 9. Changes in salt marsh platform elevation in (a) and (b), MHW in (c) and (d), and biomass density in (e) and (f) are displayed, for the low SLR (11 cm) and the high SLR (48 cm) scenarios respectively, for locations of low, medium, and high productivity as shown in Fig. 1d (indicated as Sites 1, 2, and 3).

4. Discussion

Geomorphic variation on the marsh platform as well as variation in marsh biomass and their interactions with tidal flow play a

key role in the spatial and temporal distribution of tidal constants, MLW and MHW, across an estuarine landscape. Tidal flow is affected because salt marsh systems increase momentum dissipation through surface friction, which is a function of vegetation

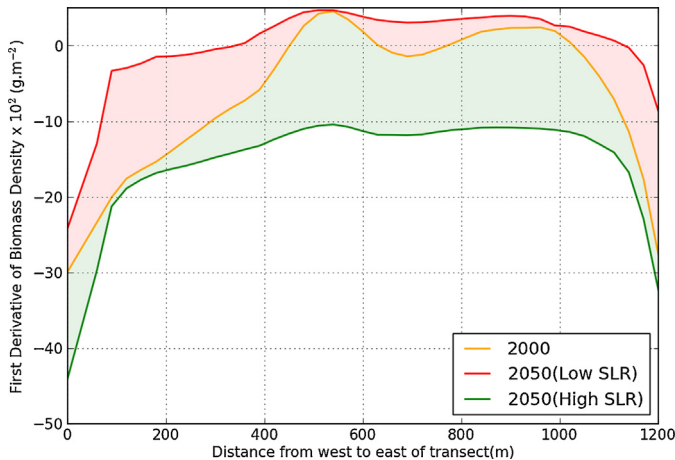


Fig. 10. Changes in the first derivative of biomass density along a transect between years 2000 and 2050. Red shaded area shows the change of the first derivative of biomass density between the year 2000 (yellow line) and the year 2050 (red line) under a low SLR (11 cm) scenario; green shaded area demonstrates the change in the first derivative of biomass between the year 2000 (yellow line) and the year 2050 (green line) under a high SLR (48 cm) scenario (For interpretation of the references to color in this figure legend, the reader is referred to the web version of this article.).

growth (Möller and Spencer, 2002; Möller et al., 1999). Furthermore, the productivity and accretion of sediment in marshes affect the total area of wetted zones and, as a result of higher SLR projections, may increase the width of the tidal creeks, and some areas that are currently covered by marshes might convert to open water. Also, as the level of water increases, water can flow with lower resistance in the tidal creeks and circulate more freely through the marshes, thus leading to less spatial variability in tidal constants within the creeks and over the marsh platform. During the high SLR scenario, water levels and flow rates increased and bottom friction was reduced. This reduced the spatial variability in MHW in the creeks and across the marshes. Further, as SLR increased, MHW in the marshes and creeks converged as energy dissipation from the marshes decreased. These energy controls are fundamental to the

geomorphological feedbacks that maintain stable marshes. At the upper end of SLR, the tidal constants are in more dynamic equilibrium, where at the lower end of SLR, the tidal constants are sensitive to subtle changes where they are in adjustment towards dynamic equilibrium.

Marsh productivity is primarily a function of relative elevation, MHW, and accretion relative to SLR. SLR affects future marsh productivity by altering elevation, relative MHW, and their distributions across the marsh platform (i.e., hydroperiod). SLR also affects the accretion rate due to the biological feedback mechanisms of the system. The Hydro-MEM model captured this relationship by updating accretion at each coupling time step based on data-derived biomass curve (MEM). Biomass density increased under the low SLR scenario as a result of the dynamic interactions between SLR and sedimentation. In this case, the low SLR scenario and the marsh system worked together to increase productivity and are in agreement with the predicted changes for salt marsh productivity in response to suggested ranges of SLR in recent study (Cadol et al., 2014).

For the low SLR scenario, the numerator in Eq. (2) decreased with increasing accretion while the denominator increased; the point on the horizontal axis of the biomass curve moved to the left, closer to the optimum part of the curve (Fig. 6). For the high SLR scenario, the numerator's growth outpaced that of the denominator in Eq. (2), and the non-dimensional depth increased to a higher value on the right side of the graph (Fig. 6). This move illustrates the decrease in salt marsh productivity from the medium to the low region on the biomass density curve. In our study, most of the locations for the year 2000 were positioned on the right side of the biomass curve (Figs. 6 and 5d). If the location is positioned on the far right or left sides of the biomass curve, the first derivative of biomass productivity is a small negative or large positive number, respectively (Fig. 6). This number characterizes the slope of the tangent line to the curve at that point on the curve. The slope will approach zero at the optimal point of the curve (parabolic maximum). Therefore, if the point transitions to the right side of the curve, the first derivative will become smaller, and if the point moves to the left side of the curve, the first derivative will become larger. Under the low SLR scenario, the first derivative showed

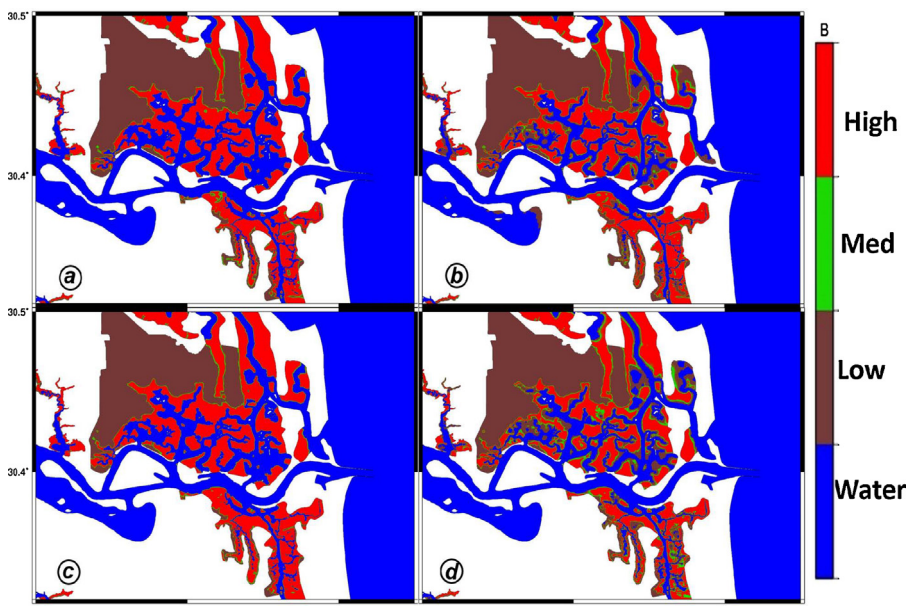


Fig. 11. Biomass density patterns between using MEM (a and c) and Hydro-MEM model (b and d) under the low SLR scenario (a and b) and the high SLR scenario (c and d). The marshes with productivity less than 370 g m^{-2} are categorized as low, between 370 g m^{-2} and 750 g m^{-2} are categorized as medium, and more than 750 g m^{-2} are categorized as high productivity.

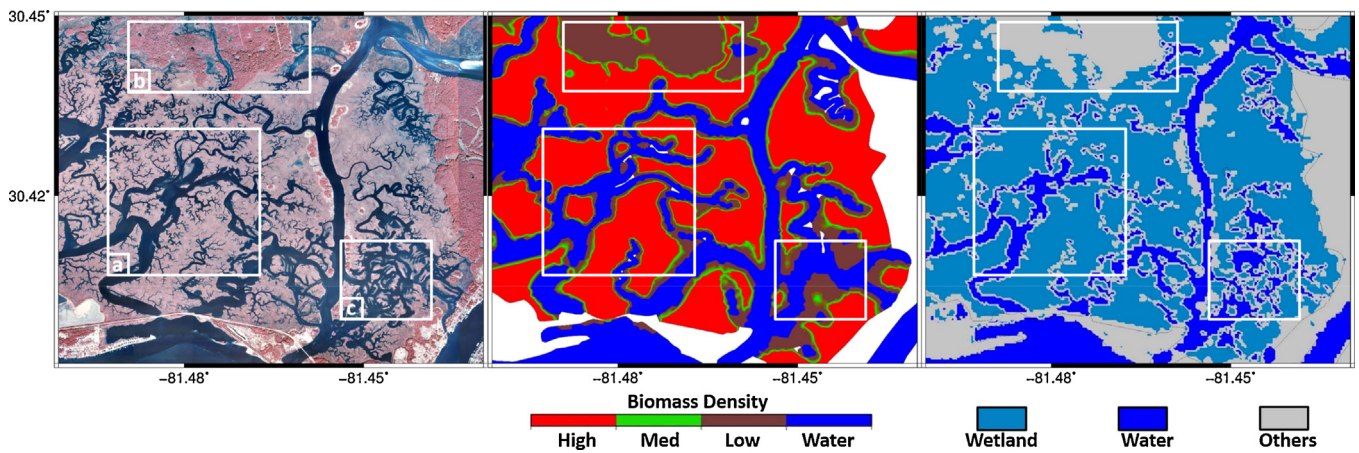


Fig. 12. Figure. Qualitative comparison maps. From left to right, infrared aerial map of Timucuan sub-region (Fig. 1d) from January 7, 1999 (USGS Digital Orthophoto Quadrangles), model generated map of open water, and low, medium, and high productivity regions, and wetland coverage area in the National Land Cover Database for the year 2001 (NLCD2001).

higher values generally approaching the optimal point (Fig. 5e). As shown in Fig. 6, the biomass density decreased under the high SLR scenario and the first derivative also decreased as it shifted to the right side of the biomass density curve (Fig. 5f).

D’Alpaos et al. (2007) found that the inorganic sedimentation portion of the accretion decreases with increasing distance from the creek, which in this study is observed throughout a majority of the marsh system, thus indicating good model performance (Fig. 7a and b). Fig. 8a and c further illustrate this finding for the transect AB (Fig. 1d), showing that the minimum accretion was in the middle of the transect (at a distance from the creeks) and the maximum was close to creeks. This model result is a consequence of the higher elevation of inland areas, and decreased inundation time of the marsh surface, rather than a result of a decrease in the mass of sediment transport.

Spatial and temporal variation in the tidal constants had a dynamic effect on accretion and also biomass density (Fig. 8a and b). The coupling between the hydrodynamic model and MEM, which included the dynamics of SLR, also helped to better capture the salt marsh’s movements toward a dynamic equilibrium. This change in condition is exemplified by the red area in Fig. 10 that depicted the movement toward the optimum point on the biomass density curve.

Although the salt marsh platform showed increased rates of accretion under high SLR, the salt marsh was not able to keep up with MHW. Salt marsh productivity declined along the edge of the creeks (Fig. 8d); if this trend were to continue, the marsh would drown. The decline depends on the underlying topography as well as the tidal metrics, neither of which are uniform across the marsh. The first derivative curve for high SLR (shaded green) in Fig. 10 illustrates a decline in biomass density; however, marshes with medium productivity due to higher accretion rates had minimal losses (Fig. 9f) and the marsh productivity remained in the intermediate level. The marshes in the high productivity zone descended to the medium zone as the marshes in the lower level were exposed to more frequent and extended inundation. As a result, in the year 2050 under the high SLR scenario, the total salt marsh area was projected to decrease, with salt marshes mostly in the medium productivity level surviving (Fig. 5c and f). The high SLR scenario also exhibits a tipping point in biomass density that occurs at different times based on low, medium or high productivity, where biomass density declines beyond the tipping point.

The complex dynamics introduced by marsh biogeomorphological feedbacks as they influence hydrodynamic, biological, and geomorphological processes across the marsh landscape can be

appreciated by examination of the time series from a few different positions within the marshes (Fig. 9). The interactions of these processes are reciprocal. That is, relative elevations affect biology, biology affects accretion of the marsh platform, which affects hydrodynamics and accretion, which affects biology, and so on. Furthermore, to add even more complexity to the biofeedback processes, the present conditions affect the future state. For example, the response of marsh platform elevation to SLR depends on the current elevation as well as the rate of SLR (Fig. 9a and b). The temporal change of accretion for the low productivity point under the high SLR scenario after 2030 can be explained by the reduction in salt marsh productivity and the resulting decrease in accretion. These marshes, which were typically near the edge of creeks, were prone to submersion under the high SLR scenario. However, the higher accretion rates for the medium and high productivity points under the high SLR compared to the low SLR scenario were due to the marsh’s adaptive capability to capture sediment. The increasing temporal rate of biomass density change for the high, medium, and low productivity points under the low SLR scenario was due to the underlying rates of change of salt marsh platform and MHW (Fig. 9). The decreasing rate of change for biomass density under the high SLR after 2030 for the medium and high productivity points, and after 2025 for the low productivity point was mainly because of the drastic change in MHW (Fig. 9f).

The sensitivity of the coupled Hydro-MEM model to the coupling time step length varied between the low and high SLR scenarios. The high SLR case required a shorter coupling time step due to the non-linear trend in water level change over time. However, the increased accuracy with a smaller coupling time step comes at the price of increased computational time. The run time for a single run of the hydrodynamic model across 120 cores (Intel Xeon quad core @ 3.0 GHz) was four wallclock hours, and with the addition of the ArcGIS portion of the Hydro-MEM model framework, the total computational time was noteworthy for this small marsh area and should be considered when increasing the number of the coupling time steps and the calculation area. Therefore, the optimum of the tested coupling time steps for the low and high SLR scenarios were determined to be 10 and 5 years, respectively.

As shown in Fig. 11 and Table 2, the incorporation of the hydrodynamic component in the Hydro-MEM model leads to different results in simulated wetland area and biomass productivity relative to the results estimated by the marsh model alone. Under the low SLR scenario, there was an 8.2% difference in predicted total wetland area between using the coupled Hydro-MEM model vs. MEM alone (Table 2), and the low and medium productivity regions were

both underestimated. Generally, MEM alone predicted higher productivity than the Hydro-MEM model results. These differences are in part attributed to the fact that such an application of MEM applies fixed values for MLW and MHW in the wetland areas and uses a bathtub approach for simulating SLR, whereas the Hydro-MEM model simulates the spatially varying MLW and MHW across the salt marsh landscape and accounts for non-linear response of MLW and MHW due to SLR (Fig. 11). Second, the coupling of the hydrodynamics and salt marsh platform accretion processes influences the results of the Hydro-MEM model.

A qualitative comparison of the model results to aerial imagery and NLCD data provided a better understanding of the biomass density model performance. The model results illustrated in areas representative of the sub-optimal, optimal and super-optimal regions of the biomass productivity curve were reasonably well captured compared with the above-mentioned ancillary data. This provided a final assessment of the model ability to produce realistic results.

The Hydro-MEM model is the first spatial model that includes (1) the dynamics of SLR and its nonlinear (Passeri et al., 2015) effects on biomass density, and (2) SLR rate by employing a time step approach in the modeling rather than using a constant value for SLR. The time step approach used here also helped to capture the complex feedbacks between vegetation and hydrodynamics. This model can be applied in other estuaries to aid resource managers in their planning for potential changes or restoration acts under climate change and SLR scenarios. The outputs of this model can be used in storm surge or hydrodynamic simulations to provide an updated friction coefficient map. The future of this model should include more complex physical processes including inflows for fluvial systems, sediment transport (Mariotti and Fagherazzi, 2010) and biologically mediated resuspension, and a realistic depiction of more accurate geomorphological changes in the marsh system.

Acknowledgments

This research is funded partially under Award No. NA10NOS4780146 from the National Oceanic and Atmospheric Administration (NOAA) Center for Sponsored Coastal Ocean Research (CSCOR) and the Louisiana Sea Grant Laborde Chair endowment. The development of MEM was supported by the grant DEB-1052636 from the National Science Foundation (NSF) to J.T. Morris. The STOKES Advanced Research Computing Center (ARCC) (webstokes.ist.ucf.edu) provided computational resources for the hydrodynamic model simulations. Earlier versions of the model were developed by James J. Angelo. The statements and conclusions do not necessarily reflect the views of NOAA-CSCOR, NSF, STOKES ARCC, Louisiana Sea Grant, or their affiliates.

References

- Allen, J.R.L., 1997. Simulation models of salt-marsh morphodynamics: some implications for high-intertidal sediment couplets related to sea-level change. *Sediment. Geol.* 113, 211–223.
- Atkinson, J., McKee Smith, J., Bender, C., 2013. Sea-level rise effects on storm surge and nearshore waves on the Texas coast: influence of landscape and storm characteristics. *J. Waterw. Port Coastal Ocean Eng.* 139, 98–117.
- Bacopoulos, P., Funakoshi, Y., Hagen, S.C., Cox, A.T., Cardone, V.J., 2009. The role of meteorological forcing on the St. Johns River (Northeastern Florida). *J. Hydrol.* 369, 55–70.
- Bacopoulos, P., Hagen, S., 2009. Tidal simulations for the Loxahatchee River Estuary (Southeastern Florida): on the influence of the Atlantic intracoastal waterway versus the surrounding tidal flats. *J. Waterw. Port Coastal Ocean Eng.* 135, 259–268.
- Bacopoulos, P., Hagen, S.C., Cox, A.T., Daily, W.R., Bratos, S.M., 2012. Observation and simulation of winds and hydrodynamics in St. Johns and Nassau Rivers. *J. Hydrol.* 420–421, 391–402.
- Bacopoulos, P., Parrish, D.M., Hagen, S.C., 2011. Unstructured mesh assessment for tidal model of the South Atlantic Bight and its estuaries. *J. Hydraul. Res.* 49, 487–502.
- Baustian, J.J., Mendelsohn Irving, A., Hester Mark, W., 2012. Vegetation's importance in regulating surface elevation in a coastal salt marsh facing elevated rates of sea level rise. *Global Change Biol.* 18, 3377–3382.
- Bilskie, M.V., Hagen, S.C., Medeiros, S.C., Passeri, D.L., 2014. Dynamics of sea level rise and coastal flooding on a changing landscape. *Geophys. Res. Lett.* 41, 927–934.
- Blum, M.D., Roberts, H.H., 2009. Drowning of the Mississippi delta due to insufficient sediment supply and global sea-level rise. *Nat. Geosci.* 2, 488–491.
- Bunya, S., Dietrich, J.C., Westerink, J.J., Ebersole, B.A., Smith, J.M., Atkinson, J.H., Jensen, R., Resio, D.T., Luettich, R.A., Dawson, C., Cardone, V.J., Cox, A.T., Powell, M.D., Westerink, H.J., Roberts, H.J., 2010. A high-resolution coupled riverine flow, tide, wind, wind wave, and storm surge model for southern Louisiana and Mississippi. Part I: model development and validation. *Mon. Weather Rev.* 138, 345–377.
- Bush, T., Houck, M., 2002. Plant fact sheet. In: Smooth Cordgrass *Spartina alterniflora* Loisel. USDA Natural Resources Conservation Service, Washington, DC.
- Cadol, D., Engelhardt, K., Elmore, A., Sanders, G., 2014. Elevation-dependent surface elevation gain in a tidal freshwater marsh and implications for marsh persistence. *Limnol. Oceanogr.* 59, 1065–1080.
- Clough, J.S., Park, R.A., Fuller, R., 2010. SLAMM 6 Beta Technical Documentation. SLAMM, Waitsfield, VT.
- Costanza, R., Ruth, M., 1998. Using dynamic modeling to scope environmental problems and build consensus. *Environ. Manage.* 22, 183–195.
- Costanza, R., Sklar, F.H., White, M.L., 1990. Modeling coastal landscape dynamics. *BioScience* 40, 91–107.
- Craft, C., Clough, J., Ehman, J., Joye, S., Park, R., Pennings, S., Guo, H., Machmuller, M., 2008. Forecasting the effects of accelerated sea-level rise on tidal marsh ecosystem services. *Front. Ecol. Environ.* 7, 73–78.
- D'Alpaos, A., Lanzoni, S., Marani, M., Rinaldo, A., 2007. Landscape evolution in tidal embayments: modeling the interplay of erosion, sedimentation, and vegetation dynamics. *J. Geophys. Res.: Earth Surf.* 112, F01008.
- D'Alpaos, A., Lanzoni, S., Mudd, S.M., Fagherazzi, S., 2006. Modeling the influence of hydroperiod and vegetation on the cross-sectional formation of tidal channels. *Estuarine Coastal Shelf Sci.* 69, 311–324.
- Dame, R., Kenny, P.D., 1986. Variability of *spartina-alterniflora* primary production in the euahine north Inlet estuary. *Mar. Ecol. Prog. Ser.* 32, 71–80.
- Darby, F., Turner, R.E., 2008. Below- and aboveground biomass of *Spartina alterniflora*: response to nutrient addition in a Louisiana salt marsh. *Estuaries Coasts* 31, 326–334.
- DeMort, C.L., 1991. The St. Johns river system. In: Livingston, R. (Ed.), *The Rivers of Florida*, vol. 83. Springer, New York, NY, pp. 97–120.
- Donnelly, J.P., Bertness, M.D., 2001. Rapid shoreward encroachment of salt marsh cordgrass in response to accelerated sea-level rise. *Proc. Natl. Acad. Sci.* 98, 14218–14223.
- ESRI, 2012. ArcMap 10.1, 10.1 ed. ESRI, Redlands, CA.
- Fagherazzi, S., Kirwan, M.L., Mudd, S.M., Guntenspergen, G.R., Temmerman, S., D'Alpaos, A., van de Koppel, J., Rybcyzk, J.M., Reyes, E., Craft, C., Clough, J., 2012. Numerical models of salt marsh evolution: ecological, geomorphic, and climatic factors. *Rev. Geophys.* 50, RG1002.
- Fitz, H.C., DeBellevue, E.B., Costanza, R., Boumans, R., Maxwell, T., Wainger, L., Sklar, F.H., 1996. Development of a general ecosystem model for a range of scales and ecosystems. *Ecol. Model.* 88, 263–295.
- Giardino, D., Bacopoulos, P., Hagen, S., 2011. Tidal Spectroscopy of the lower St. Johns river from a high-resolution shallow water hydrodynamic model. *Int. J. Ocean Climate Syst.* 2, 1–18.
- Hagen, S., Morris, J., Bacopoulos, P., Weishampel, J., 2013. Sea-level rise impact on a salt marsh system of the lower St. Johns river. *J. Waterw. Port Coastal Ocean Eng.* 139, 118–125.
- Halpin, P.M., 2000. Habitat use by an intertidal salt-marsh fish: trade-offs between predation and growth. *Mar. Ecol. Prog. Ser.* 198, 203–214.
- Homer, C., Dewitz, J., Fry, J., Coan, M., Hossain, N., Larson, C., Herold, N., McKerrow, A., VanDriel, J.N., Wickham, J., 2007. Completion of the 2001 national land cover database for the conterminous United States. *Photogramm. Eng. Remote Sens.* 73, 337.
- Hopkinson, C.S., Gosselink, J.G., Parrondo, R.T., 1980. Production of coastal Louisiana marsh plants calculated from phenometric techniques. *Ecology* 61, 1091–1098.
- Hutchinson, G.E., 1957. Cold spring harbor symposium on quantitative biology. *Concluding remarks* 22, 417–427.
- Jørgensen, S.E., Fath, B.D., 2011a. 10-Structurally dynamic models. In: Sven Erik, J., Brian, D.F. (Eds.), *Developments in Environmental Modelling*, vol. 23. Elsevier, Amsterdam, pp. 309–346.
- Jørgensen, S.E., Fath, B.D., 2011b. 11-Spatial modelling. In: Sven Erik, J., Brian, D.F. (Eds.), *Developments in Environmental Modelling*, vol. 23. Elsevier, Amsterdam, pp. 347–368.
- Kirwan, M.L., Guntenspergen, G.R., 2012. Feedbacks between inundation, root production, and shoot growth in a rapidly submerging brackish marsh. *J. Ecol.* 100, 764–770.
- Kirwan, M.L., Murray, A.B., 2007. A coupled geomorphic and ecological model of tidal marsh evolution. *Proc. Natl. Acad. Sci. U.S.A.* 104, 6118–6122.
- Knutson, P., 1987. *Role of Coastal Marshes in Energy Dissipation and Shore Protection, The Ecology and Management of Wetlands*. Springer, US, pp. 161–175.
- Leonard, L.A., Croft, A.L., 2006. The effect of standing biomass on flow velocity and turbulence in *Spartina alterniflora* canopies. *Estuarine Coastal Shelf Sci.* 69, 325–336.
- Leonard, L.A., Luther, M.E., 1995. Flow hydrodynamics in tidal marsh canopies. *Limnol. Oceanogr.* 40, 1474–1484.

- Luettich, R.A., Westerink, J.J., Scheffner, N.W., 1992. ADCIRC: an advanced three-dimensional circulation model for shelves, coasts, and estuaries. I: Theory and methodology of ADCIRC-2DD1 and ADCIRC-3DL. In: Technical Rep. No. DRP-92-6. U.S. Army Engineer Waterways Experiment Station, Vicksburg, MS.
- Marani, M., Da Lio, C., D'Alpaos, A., 2013. Vegetation engineers marsh morphology through multiple competing stable states. *Proc. Natl. Acad. Sci. U.S.A.* 110, 3259–3263.
- Mariotti, G., Fagherazzi, S., 2010. A numerical model for the coupled long-term evolution of salt marshes and tidal flats. *J. Geophys. Res.: Earth Surf.* (2003–2012) 115, Article Number: F01004 <http://onlinelibrary.wiley.com/doi/10.1029/2009JF001326/full>.
- Martin, J.F., Reyes, E., Kemp, G.P., Mashriqui, H., Day, J.W., 2002. Landscape modeling of the Mississippi Delta: using a series of landscape models, we examined the survival and creation of Mississippi Delta marshes and the impact of altered riverine inputs, accelerated sea-level rise, and management proposals on these marshes. *BioScience* 52, 357–365.
- Martin, J.F., White, M.L., Reyes, E., Kemp, G.P., Mashriqui, H., Day, J.J.W., 2000. PROFILE: evaluation of coastal management plans with a spatial model: Mississippi Delta, Louisiana, USA. *Environ. Manage.* 26, 117–129.
- McKee, K.L., Patrick, W., 1988. The relationship of smooth cordgrass (*Spartina alterniflora*) to tidal datums: a review. *Estuaries* 11, 143–151.
- Medeiros, S.C., Hagen, S.C., 2013. Review of wetting and drying algorithms for numerical tidal flow models. *Int. J. Numer. Methods Fluids* 71, 473–487.
- Möller, I., Spencer, T., 2002. Wave dissipation over macro-tidal saltmarshes: effects of marsh edge typology and vegetation change. *J. Coastal Res.* 36, 506–521.
- Möller, I., Spencer, T., French, J.R., Leggett, D.J., Dixon, M., 1999. Wave transformation over salt marshes: a field and numerical modelling study from North Norfolk, England. *Estuarine Coastal Shelf Sci.* 49, 411–426.
- Morris, J., 1995. The mass balance of salt and water in intertidal sediments: results from North Inlet, South Carolina. *Estuaries* 18, 556–567.
- Morris, J., 2007. Ecological engineering in intertidal saltmarshes. *Hydrobiologia* 577, 161–168.
- Morris, J.T., 2015. Marsh equilibrium theory. In: ICI Spartina Conference Proceedings. University of Rennes Press, Vicksburg, MS (In Press).
- Morris, J.T., Sundareshwar, P.V., Nietch, C.T., Kjerfve, B., Cahoon, D.R., 2002. Responses of coastal wetlands to rising sea level. *Ecology* 83, 2869–2877.
- Morris, J.T., Sundberg, K., Hopkinson, C.S., 2013. Salt marsh primary production and its responses to relative sea level and nutrients in estuaries at Plum Island, Massachusetts, and North Inlet, South Carolina, USA. *Oceanography* 26, 78–84.
- Mudd, S.M., D'Alpaos, A., Morris, J.T., 2010. How does vegetation affect sedimentation on tidal marshes? Investigating particle capture and hydrodynamic controls on biologically mediated sedimentation. *J. Geophys. Res.: Earth Surf.* 115, F03029.
- Mudd, S.M., Fagherazzi, S., Morris, J.T., Furbish, D.J., 2004. Flow, sedimentation, and biomass production on a vegetated salt marsh in South Carolina: toward a predictive model of marsh morphologic and ecologic evolution. *The Ecogeomorphology of Tidal Marshes*, vol. 59. AGU, Washington, DC, pp. 165–188.
- Nyman, J.A., DeLaune, R., Roberts, H., Patrick Jr., W., 1993. Relationship between vegetation and soil formation in a rapidly submerging coastal marsh. *Mar. Ecol. Prog. Ser. (Oldendorf)* 96, 269–279.
- Nyman, J.A., Walters, R.J., DeLaune, R.D., Patrick Jr., W.H., 2006. Marsh vertical accretion via vegetative growth. *Estuarine Coastal Shelf Sci.* 69, 370–380.
- Park, R.A., Armentano, T.V., Cloonan, C.L., 1986. Predicting the effects of sea level rise on coastal wetlands. Effects of Changes in Stratospheric Ozone and Global Climate, vol. 4. U.S. Environmental Protection Agency, pp. 129–152.
- Park, R.A., Trehan, M.S., Mause, P.W., Howe, R.C., Titus, J.G., 1989. The Effects of Sea Level Rise on US Coastal Wetlands and Lowlands. Office of Policy, Planning and Evaluation, US Environmental Protection Agency, Washington, DC.
- Parris, A., Bromirski, P., Burkett, V., Cayan, D., Culver, M., Hall, J., Horton, R., Knuuti, K., Moss, R., Obeysekera, J., Sallenger, A., Weiss, J., 2012. Global Sea Level Rise Scenarios for the US National Climate Assessment. NOAA Tech Memo OAR CPO, Silver Spring, MD, pp. 1–37.
- Passeri, D.L., Hagen, S.C., Medeiros, S.C., Bilskie, M.V., 2015. Impacts of historic morphological changes and sea level rise on tidal hydrodynamics in the Grand Bay, Mississippi estuary. *Estuarine Coastal Shelf Sci.* (Submitted) <http://onlinelibrary.wiley.com/doi/10.1002/2015EF000298/full>.
- Patrick, W.H., DeLaune, R.D., 1990. Subsidence accretion and sea level rise in south San Francisco Bay marshes. *Limnol. Oceanogr.* 35, 1389–1395.
- Pennings, S.C., Bertness, M.D., 2001. Salt marsh communities. *Mar. Community Ecol.*, 289–316.
- Reed, D.J., 1990. The impact of sea-level rise on coastal salt marshes. *Prog. Phys. Geogr.* 14, 465–481.
- Reed, D.J., 1995. The response of coastal marshes to sea-level rise: survival or submergence? *Earth Surf. Processes Landforms* 20, 39–48.
- Reyes, E., White, M.L., Martin, J.F., Kemp, G.P., Day, J.W., Aravamuthan, V., 2000. Landscape modeling of coastal habitat change in the Mississippi Delta. *Ecology* 81, 2331–2349.
- Schile, L.M., Callaway, J.C., Morris, J.T., Stralberg, D., Parker, V.T., Kelly, M., 2014. Modeling tidal marsh distribution with sea-level rise: evaluating the role of vegetation, sediment, and upland habitat in marsh resiliency. *PLoS ONE* 9, e88760.
- Schubauer, J.P., Hopkinson, C.S., 1984. Above- and belowground emergent macrophyte production and turnover in a coastal marsh ecosystem, Georgia. *Limnol. Oceanogr.* 29, 1052–1065.
- Shepard, C.C., Crain, C.M., Beck, M.W., 2011. The protective role of coastal marshes: A systematic review and meta-analysis. *PLoS ONE* 6, e27374.
- Silliman, B.R., Bertness, M.D., 2002. A trophic cascade regulates salt marsh primary production. *Proc. Natl. Acad. Sci.* 99, 10500–10505.
- Sklar, F.H., Costanza, R., Day Jr., J.W., 1985. Dynamic spatial simulation modeling of coastal wetland habitat succession. *Ecol. Model.* 29, 261–281.
- Stralberg, D., Brennan, M., Callaway, J.C., Wood, J.K., Schile, L.M., Jongsomjit, D., Kelly, M., Parker, V.T., Crooks, S., 2011. Evaluating tidal marsh sustainability in the face of sea-level rise: a hybrid modeling approach applied to San Francisco Bay. *PLoS ONE* 6, e27388.
- Tambroni, N., Seminara, G., 2012. A one-dimensional eco-geomorphic model of marsh response to sea level rise: wind effects, dynamics of the marsh border and equilibrium. *J. Geophys. Res.: Earth Surf.* 117, F03026.
- Temmerman, S., Bouma, T.J., Van de Koppel, J., Van der Wal, D., De Vries, M.B., Herman, P.M.J., 2007. Vegetation causes channel erosion in a tidal landscape. *Geology* 35, 631–634.
- Temmerman, S., Govers, G., Meire, P., Wartel, S., 2003. Modelling long-term tidal marsh growth under changing tidal conditions and suspended sediment concentrations, Scheldt estuary, Belgium. *Mar. Geol.* 193, 151–169.
- Thomas, R.E., Johnson, M.F., Frostick, L.E., Parsons, D.R., Bouma, T.J., Dijkstra, J.T., Eiff, O., Gobert, S., Henry, P.-Y., Kemp, P., McLellan, S.J., Moulin, F.Y., Myrhaug, D., Neyts, A., Paul, M., Penning, W.E., Puijalon, S., Rice, S.P., Stanica, A., Tagliapetra, D., Tal, M., Tørum, A., Voudoukouas, M.I., 2014. Physical modelling of water, fauna and flora: knowledge gaps, avenues for future research and infrastructural needs. *J. Hydraul. Res.* 52, 311–325.
- Thorne, K.M., Elliott-Fisk, D.L., Wyllie, G.D., Perry, W.M., Takekawa, J.Y., 2014. Importance of biogeomorphic and spatial properties in assessing a tidal salt marsh vulnerability to sea-level rise. *Estuaries Coasts* 37, 941–951.
- Townend, I., Fletcher, C., Knappen, M., Rossington, K., 2011. A review of salt marsh dynamics. *Water Environ. J.* 25, 477–488.
- Turner, R.E., Swenson, E.M., Milan, C.S., 2000. Organic and inorganic contributions to vertical accretion in salt marsh sediments. In: Weinstein, M., Kreger, D. (Eds.), Concepts and Controversies in Tidal Marsh Ecology. Springer, Netherlands, pp. 583–595.
- United States Army Corps of Engineers, 2011. Sea-level Change Considerations for Civil Works Programs EC 1165-2-212. United States Army Corps of Engineers.
- United States National Park Service (Denver Service Center), 1996. Timucuan Ecological and Historic Preserve, Florida: General Management Plan, Development Concept Plans. US National Park Service, Denver Service Center.
- Walton Jr., T.L., 2007. Projected sea level rise in Florida. *Ocean Eng.* 34, 1832–1840.
- Warren, R.S., Niering, W.A., 1993. Vegetation change on a northeast tidal marsh: interaction of sea-level rise and marsh accretion. *Ecology* 74, 96–103.